ULTRAVIOLET ASTRONOMY IN THE XXI CENTURY

e-Workshop 2020 – October 27-29

JcUVa

Analyzing the Bulge of M31 in the ASTROSAT Ultraviolet Data

Cole Morgan[1], Denis Leahy[1], Joe Postma[1], Megan Buick[1], Luciana Bianchi[2], John Hutchings[3]

[1]Department of Physics & Astronomy, University of Calgary, [2]John Hopkins University, [3]Herzberg Institute for Astrophysics

UNIVERSITY OF CALGARY

Abstract

AstroSat has carried out a survey of M31 with the UVIT telescope from 2017 to 2019. The central bulge of M31 was observed in NUV N2 (2750-2850 A), NUV B15 (2000-2400 A), FUV Silica (1600-1850 A), FUV Sapphire (1450-1750 A), and FUV CaF2 (1200-1800 A) filters. A radial profile analysis, averaged along elliptical contours which approximate the bulge shape, was carried out in each filter. The profiles are fit well by Sersic profiles, apart from the inner 4 arcseconds of the core which have a significant excess in all filters. The UV colors of the bulge are found to change systematically with radius, such that the center of the bulge is bluer (hotter). The FUV increases more dramatically than the NUV.

Introduction and Data Extraction

After processing in CCDLab, The UVIT instrument aboard the ASTROSAT spacecraft has produced 9 images of the bulge of M31 across 5 UV filters: NUVN2, NUVB15, FUVSilica, FUVSapphire, and FUVCaF2. Elliptical profiles were calculated in all 9 images, and are shown below in figure 1. The ellipse parameters used in all fields were based on CCDLab's 2D elliptical Gaussian fit of the inner 50" around the core. An elliptical profile is a radial profile averaged over all angles which accounts for the apparent ellipticity of the bulge. The flux in each pixel within concentric, 0.4" pixel wide elliptical annuli were averaged to produce each data point. 240 such ellipses were measured, from the central core out to 164" along the major axis. Examples of these ellipses are drawn in figure 4.

The profiles generally follow a Sersic shape, with lower wavelength filters having higher indices. Indices range from 2.3 in the NUV to 5.3 in the FUV.

The innermost 5" have a significant excess above a pure sersic profile in all filters. This excess is more pronounced in the FUV than the NUV
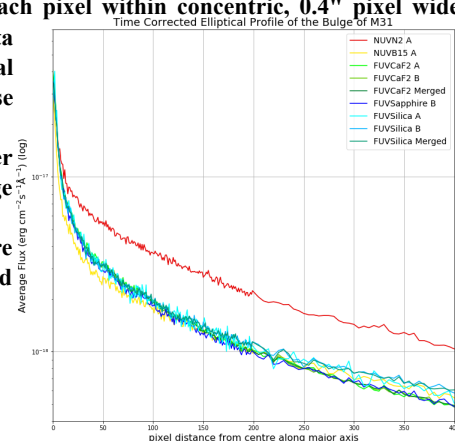

Fig. 1. Plot of the elliptical profiles from all 9 images of the bulge.

Fitting Elliptical Profiles

Chi squared analysis was used to fit analytic functions to the elliptical profiles. The outer data was fit well by Sersic functions, with the index increasing with wavelength. A second Sersic function, Gaussian, and point source function were fit to the central excess. The excess is likely not due to the UVIT instrument's point source spread, as it does not have a significant effect beyond 10 pixels from a source, as shown in figure 2 below. The cause of this excess would require a greater angular resolution than the UVIT telescope observes to study in detail.

Table 1 contains the best fit parameters of each fit type when excluding the inner 10 pixels. The double Sersic fit and Sersic plus Gaussian fit proved to be somewhat better than the single Sersic. The Sersic plus Gaussian is best overall, though it is only marginally better than the double Sersic in most filters.

Table 1. Table of best fit parameters when excluding the inner 10 pixels. Fits were found using the curve_fit function in the python module sciPy. Each fit was done a few thousand times with different starting values each time to ensure the true minimum was found. Note: DOF = degrees of freedom.
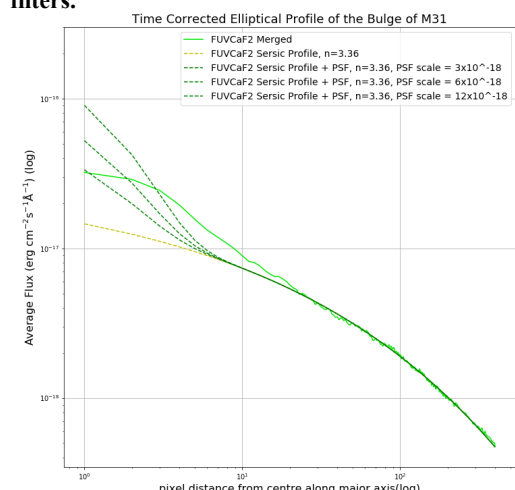
Single Sersic Fit	NUVN2	NUVB15	FUVSilica	FUVSapphire	FUVCaF2
I0	1.77E-17	2.27E-17	1.49E-16	8.86E-17	5.6E-17
k	0.228	0.765	1.98	1.53	1.13
n	2.38	3.77	5.82	4.90	4.16
Chi^2	278.1	295.5	363.3	401.8	958.7
Equation	$y = I0 \cdot exp(-k \cdot x^{\frac{1}{n}})$				
DOF	227				
Double Sersic Fit	NUVN2	NUVB15	FUVSilica	FUVSapphire	FUVCaF2
I01	3.67E-16	2.56E-16	2.16E-16	2.17E-16	3.68E-16
k1	2.26	0.614	2.12	2.11	2.34
n1	5.30	1.27	5.47	5.32	5.03
I02	1.71E-17	2.19E-17	5.25E-17	3.98E-17	4.41E-17
k2	0.217	0.742	1.20	0.972	0.966
n2	2.34	3.72	4.52	3.96	3.88
Chi^2	261.9	293.3	333.7	358.5	804
Equation	$y = I01 \cdot exp(-k1 \cdot x^{\frac{1}{n1}}) + I02 \cdot exp(-k2 \cdot x^{\frac{1}{n2}})$				
DOF	224				
Sersic + Gaussian Fit	NUVN2	NUVB15	FUVSilica	FUVSapphire	FUVCaF2
I0	1.64E-17	1.36E-17	6.19E-17	4.27E-17	2.96E-17
k	0.2	0.473	1.32	1.02	0.727
n	2.28	3.1	4.72	4.05	3.45
a	5.61E-18	2.05E-18	2.12E-18	2.14E-18	2.61E-18
c	6.19	10	9.69	10	10
Chi^2	261.1	253.9	333.2	361	723.6
Equation	$y = I0 \cdot exp(-k \cdot x^{\frac{1}{n}}) + a \cdot exp(\frac{-x^2}{2c^2})$				
DOF	225				

Fig. 2. Plot of the FUV CaF2 profile with sersic profile and sersic + PSF plotted alongside.
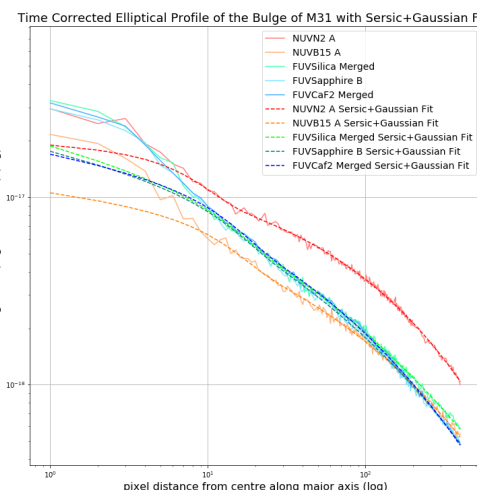

Fig. 3. Plots of the Sersic +Gaussian fits from Table 1, alongside the data with logarithmic x-axis. Note again that the inner 10 pixels were excluded from the fits, so these do not fully account for the excess.
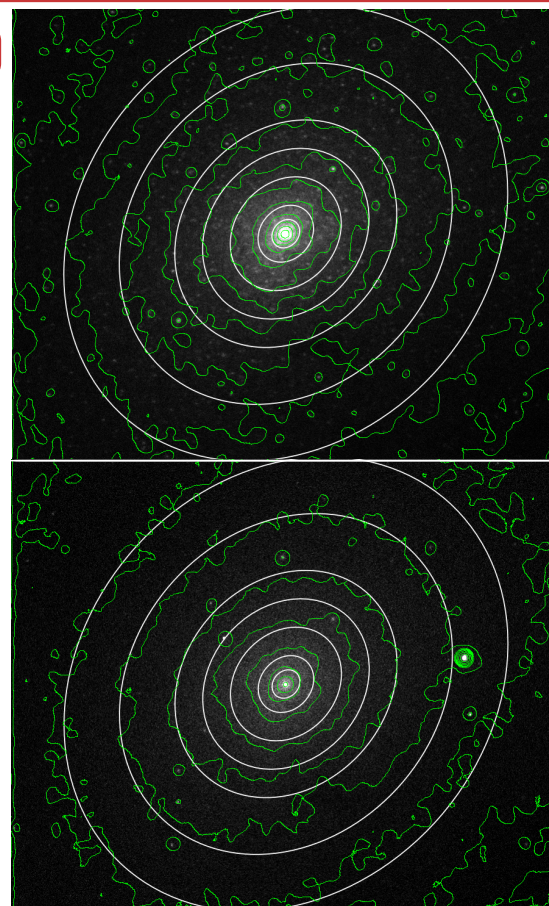

Fig. 4. The Bulge of M31 in the FUV (top) and NUV (bottom). Contours (green) and ellipses used to generate the elliptical profiles (white) are drawn on top. The images are 370" by 330" across. The bright point to the right in the NUV is a bright (possibly foreground) star.

Shape Changes

CCDLab was used to fit elliptical gaussian functions to increasingly larger portions of the bulge. Figures 5 and 6 show the ellipticity (a/b) and inclination (φ) as a function of major axis (a). Inclination is measured in radians from the image's horizontal axis.

The bulge's apparent inclination changes smoothly with increasing major axis, reaching a peak at 50 pixels (20"). It then slowly decreases outwards, implying an apparent clockwise "swirl" in the bulge.

The ellipticity seems to change differently in the NUV vs the FUV. Figure 5 shows that the shorter wavelength filters have generally higher ellipticity, with an the peak occurring sooner in the NUV than the FUV.

Contour plots such as in figure 4 seem to show a more circular core, which is a likely cause for the steep rise in inclination. Small bounding box sizes also yielded erratic results, likely also a result of an apparently mostly circular inner core. For this reason, data from bounding boxes below 40 pixels half width are not shown, nor considered in our analysis. This corresponds to a cutoff around 10 pixels along the major axis.
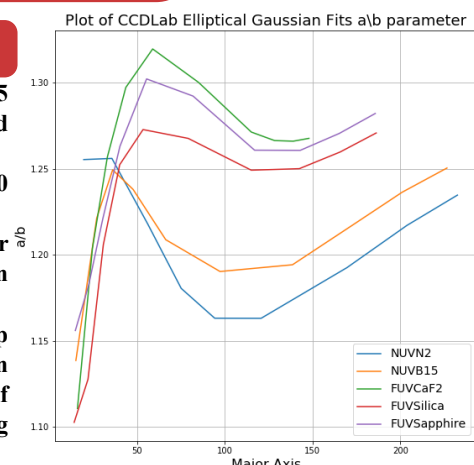
Colour Changes

A colour-colour diagram (Figure 7) was produced using the elliptical profiles in the NUVN2, NUVB15, and CaF2 (merged) images. The colours on the diagram are based entirely on the semi-major axes of the corresponding ellipses, and are designed to show which points are near the centre. NUVN2 is the longest ultraviolet wavelength available (280 nm), while FUVCaF2 is the shortest (150 nm). Points nearest the centre have a much greater ratio of FUVCaF2 flux to NUVB15 flux than those further out, while having a similar ratio of NUVB15 to NUVN2. Thus the ultraviolet colour of the bulge becomes "bluer" towards the core.

The colours of black bodies of varying interstellar extinction (Av) and temperature are plotted alongside the data, to act as a point of reference for the colour-temperature of the bulge in the UV. The observed colours are consistent with black bodies between 9500-11000K, with interstellar extinction between 0.4 and 0.7.

Similarly, stellar atmosphere models from *Castelli and Kurucz, 2004* are also plotted. The data most closely matches the colours of stars between 8500-9000K, with somewhat higher extinction between 0.7 and 1.1.
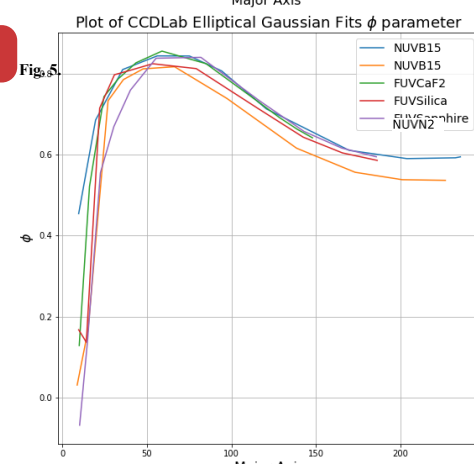

Fig. 5.

Fig. 6. Note that each filter in these plots has the same number of data points. The controlled variable in each was the bounding box size in which CCDLab performed the elliptical gaussian fit. Both the x and y axes are dependent on this value, so some filters appear to stop short of others. The FUV tended to have smaller major axes, likely as a result of the steeper increase in brightness towards the core in the FUV compared to the NUV. (see Conclusion).
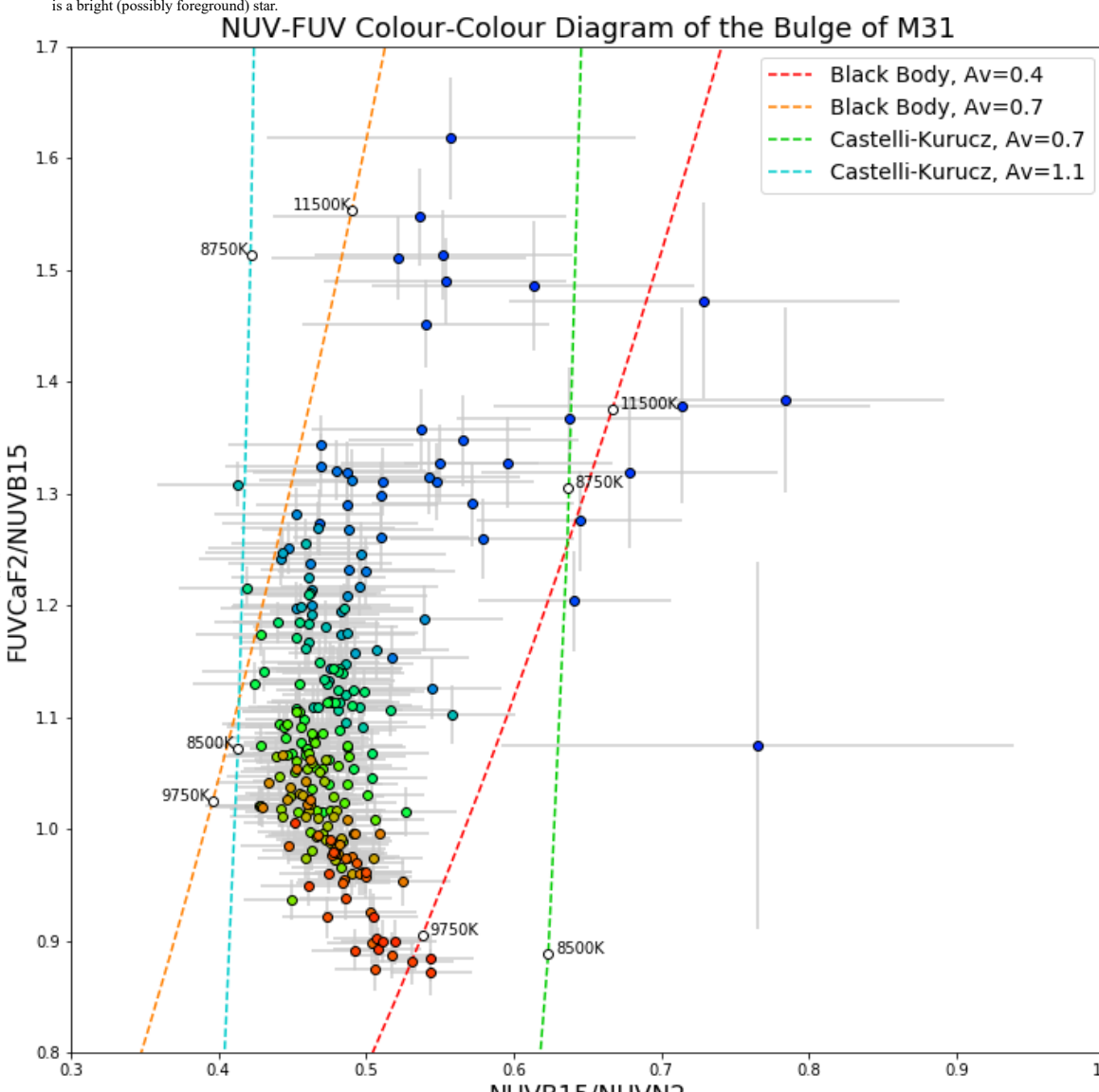

Fig. 7. The colour of points on this plot are dependent on the semi major axis of the corresponding ellipse. Bluer points are smaller ellipses, while redder points are larger. Errors are largest near the centre as a result of there being fewer pixels being averaged in the smaller ellipses.

Conclusions

The bulge of M31 primarily follows a Sersic function at all wavelengths, though is not perfectly described as such. The innermost core contains a significant, extended, broad-spectrum ultraviolet source which is difficult to study at this angular resolution.

The shape of the bulge on the sky is much more complicated than a single elliptical Gaussian can describe. The inclination changes with radius, but is quite uniform across the UV spectrum. The ellipticity changes with both distance and wavelength, with the highest ellipticity at short wavelength and medium distance. This and contour plots show the core is more circular than the rest of the bulge.

Finally, the bulge becomes significantly "bluer" towards the centre. This is seen most easily in the colour-colour diagram. *Leahy et. al., 2018* found evidence for a young bright stellar population in M31's bulge, and this combined with unresolved stellar remnants and other evolved stars are possible causes of the colour change.

The increasing steepness of the Sersic fits and increasing ellipticity with lower wavelength may be caused by the same phenomenon. If the material producing the FUV excess were more laterally compressed than the NUV (having higher ellipticity), then one would expect a steeper gradient across a larger range of angles, resulting in a steeper gradient in the average too. The reason for this is illustrated in figure 8. A phenomenon like this does not on its own explain the magnitude of colour change observed, only the rate at which it occurs towards the core.
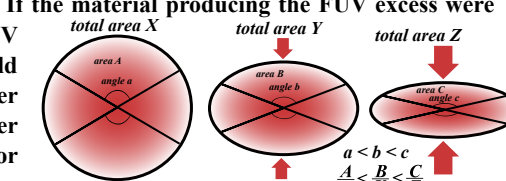

Fig. 8. As an elliptical gaussian is compressed, the gradient is steepest along the minor axis. If one considered the area contained by lines of equal gradient, this area becomes a larger proportion of the total and has a steeper gradient as the ellipticity increases. Thus the average gradient increases with ellipticity.

Acknowledgements

References

Tandon et. al. In-orbit Calibrations of the Ultraviolet Imaging Telescope. 2017.
Leahy et. al. ASTROSAT/UVIT Survey of M31, First Results: UV-bright Stars in the Bulge. 2018.
J. Postma and D. Leahy. CCDLAB: A Graphical User Interface FITS Image Data Reducer, Viewer, and Canadian UVIT Data Pipeline. 2017.
F. Castelli and R.L. Kurucz. New Grids of ATLAS9 Model Atmospheres. 2004.
K. Lockhart. A High Resolution View of Galactic Centers. 2017.